Applied Catalysis B: Environmental 162 (2015) 34–44

Contents lists available at ScienceDirect

Applied Catalysis B: Environmental

journal homepage: www.elsevier.com/locate/apcatb

Degradation of trimethoprim antibiotic by UVA photoelectro-Fenton process mediated by Fe(III)–carboxylate complexes

Francisca C. Moreira [a], Rui A.R. Boaventura [a], Enric Brillas [b], Vítor J.P. Vilar [a,*]

[a] LSRE—Laboratory of Separation and Reaction Engineering, Associate Laboratory LSRE/LCM, Departamento de Engenharia Química, Faculdade de Engenharia, Universidade do Porto, Rua Dr. Roberto Frias, 4200-465 Porto, Portugal
[b] Laboratori d'Electroquímica dels Materials i del Medi Ambient, Departament de Química Física, Facultat de Química, Universitat de Barcelona, Martí i Franquès 1-11, 08028 Barcelona, Spain

ARTICLE INFO

Article history:
Received 4 April 2014
Received in revised form 2 June 2014
Accepted 6 June 2014
Available online 14 June 2014

Keywords:
UVA photoelectro-Fenton
Ferricarboxylates
Near-neutral pH
Trimethoprim

ABSTRACT

A UVA photoelectro-Fenton (PEF) process mediated by Fe(III)–carboxylate complexes was applied to the removal of trimethoprim (TMP) antibiotic from water using a 2.2 L lab-scale flow plant equipped with a double compound parabolic collector (CPC) and an electrochemical cell composed of a boron-doped diamond (BDD) anode and a carbon–PTFE air-diffusion cathode. The presence of Fe(III)–carboxylate complexes enhances the regeneration of Fe^{3+} to Fe^{2+}, allows to maintain iron in solution at higher pH values and can decrease the formation of Fe(III)–sulfate, Fe(III)–chloride and some Fe(III)–pollutants complexes. First, the efficiency of different carboxylate ligands like oxalate, citrate, tartrate and malate was assessed, followed by the application of various initial Fe(III)-to-carboxylate molar ratios and pH values. The PEF process with Fe(III)–oxalate, Fe(III)–citrate and Fe(III)–tartrate complexes revealed similar ability to degrade the antibiotic solution with the employment of 1:3, 1:1 and 1:1 Fe(III)-to-carboxylate molar ratios, respectively, and using pH of 4.5, Fe^{3+} concentration of 2.0 mg L^{-1} (total iron emission limit for the discharge of treated effluents according to the Portuguese legislation), current density of 5 mA cm^{-2} and 20 °C. The PEF process mediated by Fe(III)–malate complexes was much less effective. 1:6 and 1:9 Fe(III)-to-oxalate molar ratios were required to yield similar TMP removal kinetics at pH 5.0 and 5.5 compared to pH 4.5, respectively. Additionally, the influence of initial TMP content and solution temperature on the PEF process with Fe(III)–carboxylate complexes was assessed and the role of the different reactive oxidizing species was clarified by the addition of scavenging agents. Generated low-molecular-weight carboxylic acids were monitored by ion-exclusion HPLC.

1. Introduction

Recently, several electrochemical advanced oxidation processes (EAOPs) have been applied to the removal of non-biodegradable organic compounds such as synthetic dyes [1,2], pesticides [3,4] and pharmaceuticals [5–7]. These techniques are based on the in situ generation of hydroxyl radicals (•OH), which are strong oxidants that can non-selectively react with organic compounds leading to their mineralization to CO_2, water and inorganic ions [8]. The most potent EAOPs use •OH both in heterogeneous and homogeneous phases, i.e. adsorbed at the anode M surface (M(•OH)) and in the solution bulk, respectively. M(•OH) is generated as intermediate from O_2 evolution from water oxidation at the anode surface via the following equation [9]:

$$M + H_2O \rightarrow M(^{\bullet}OH) + H^+ + e^- \quad (1)$$

The production of •OH in the solution bulk is achieved through the addition of low amounts of Fe^{2+} to the solution to react with H_2O_2 according to Fenton's reaction (2) [10]:

$$Fe^{2+} + H_2O_2 \rightarrow Fe^{3+} + {}^{\bullet}OH + OH^- \quad (2)$$

The H_2O_2 employed in Eq. (2) can be obtained by direct electro generation at the cathode from the two-electron cathodic reduction of injected O_2 via Eq. (3) [11]:

$$O_{2(g)} + 2H^+ + 2e^- \rightarrow H_2O_2 \quad (3)$$

Good efficiencies for H_2O_2 generation from Eq. (3) have been reported for various carbonaceous cathodes, with emphasis on carbon-felts [12–14] and carbon–PTFE gas (O_2 or air) diffusion electrodes [6,15,16]. Moreover, Fe^{2+} is continuously regenerated by

* Corresponding author. Tel.: +351 918257824; fax: +351 225081674.
E-mail address: vilar@fe.up.pt (V.J.P. Vilar).

http://dx.doi.org/10.1016/j.apcatb.2014.06.008
0926-3373/

the cathodic reduction of Fe^{3+} to Fe^{2+} from Eq. (4), with further improvement of Fenton's reaction (2) [17].

$$Fe^{3+} + e^- \rightarrow Fe^{2+} \quad (4)$$

Among EAOPs based on Fenton's reaction, UVA photoelectro-Fenton (PEF) and solar photoelectro-Fenton (SPEF) methods acquired especial relevance as they count on the use of UVA artificial light and sunlight, respectively, which yield higher degradation rates since: (i) the photo reduction of photoactive Fe(III)–hydroxy complexes as $FeOH^{2+}$ from Eq. (5) provides Fe^{3+} regeneration to Fe^{2+} and production of more $^{\bullet}OH$ [18]; and (ii) complexes formed between Fe^{3+} and some organic intermediates, especially Fe(III)–carboxylate complexes, are able to absorb in the UV–vis region and therefore can be photodecarboxylated through a ligand-to-metal charge transfer (LMCT) according to the general Eq. (6), providing a quicker pathway for Fe^{3+} regeneration to Fe^{2+} with formation of weak oxidizing species such as $O_2^{\bullet-}$, $CO_2^{\bullet-}$ and H_2O_2 [19–22].

$$FeOH^{2+} + h\nu \rightarrow Fe^{2+} + {}^{\bullet}OH \quad (5)$$

$$[Fe^{3+}(RCO_2)]^{2+} + h\nu \rightarrow Fe^{2+} + CO_2 + R^{\bullet} \quad (6)$$

Some of the main drawbacks for the real application of PEF and SPEF processes are: (i) their optimal operation at acid pH with consequent need for initial acidification and final neutralization steps—pH 2.8 is frequently postulated as optimal since at this pH in most systems precipitation does not take place yet and the dominant iron species in solution is $FeOH^{2+}$, the most photoactive Fe(III)–hydroxy complex [23,24]; (ii) the requirement of excess iron removal at the end of the reaction in order to comply with the discharge limits; (iii) the formation of strong and stable complexes between Fe^{3+} and some pollutants, limiting the photoreduction of Fe^{3+} and then the overall efficiency of the process [25]; and (iv) the adverse influence of the presence of inorganic anions as sulfate and chloride mainly due to the formation of Fe(III) complexes such as $FeSO_4^+$ and $Fe(SO_4)_2^-$, $FeCl^+$, $FeCl^{2+}$ and $FeCl_2^+$, which are much less photoactive than $FeOH^{2+}$ [26], and also in virtue of $^{\bullet}OH$ scavenging along with the formation of less reactive species as $SO_4^{\bullet-}$, $Cl^{\bullet}$ and $Cl_2^{\bullet-}$ when compared with $^{\bullet}OH$ [27–29].

Regarding the potentialities of Fe(III)–carboxylate complexes, the efficiency of PEF and SPEF systems may be improved by an initial input of some carboxylic acids along with Fe^{3+} addition to form these complexes, which conveys in a quicker Fe^{3+} regeneration to Fe^{2+} by Eq. (6) from the very first times of reaction. The quantum yield for Fe^{2+} formation in Eq. (6) depends on various parameters including the nature of the carboxylate ligand, Fe(III)-to-ligand ratio, wavelength of the light source and pH [30]. Fe(III)–oxalate, Fe(III)–citrate, Fe(III)–tartrate and Fe(III)–malate complexes have been pointed out as some of the main Fe(III)–carboxylate complexes with the highest quantum yields for Fe^{2+} generation, exhibiting much higher quantum yields for Fe^{2+} formation than $FeOH^{2+}$ complex [22,30,31]. Furthermore, it could be expected that the use of Fe(III)–carboxylate complexes may solve two of the main limitations of PEF and SPEF since: (i) their presence permits iron in solution at higher pH, thus extending the reaction optimal pH range from acid to neutral values and enabling the treatment of real waters and wastewaters without acidification and neutralization steps with the consequent minimization of costs [32]; and (ii) Fe(III)–sulfate and Fe(III)–chloride complexes [33] and some Fe(III)–pollutants complexes [25,33–35] exhibit lower formation constants than Fe(III)–carboxylate complexes, and then the formation of these undesirable species can be avoided with simultaneous increase of Fe^{3+} regeneration to Fe^{2+}.

Trimethoprim (TMP, 2,4-diamino-5-(3,4,5-trimethoxybenzyl)pyrimidine) is an antibiotic commonly prescribed alone or in combination with a sulfonamide (e.g. sulfamethoxazole, sulfadiazine or sulfamoxole) for the treatment of specific bacterial infection, including gastro, respiratory and urinary infections [36]. This antibiotic has been detected in surface waters, wastewater treatment plants (WWTPs) influents and effluents and hospital effluents at the level of ng L^{-1} to μg L^{-1} (0.003–4.30 μg L^{-1}) [37,38]. Since TMP cannot be degraded by conventional treatments, EAOPs can be a useful solution for its removal from waters.

This paper presents a study on the degradation of 68.9 μM (20.0 mg L^{-1}) TMP solutions in 50 mM Na_2SO_4, in terms of antibiotic concentration and dissolved organic carbon (DOC) decays, using a PEF process mediated by Fe(III)–carboxylate complexes. The experiments were performed in a 2.2 L lab-scale flow plant equipped with a double compound parabolic collector (CPC) and an electrochemical reactor containing a boron-doped diamond (BDD) anode and a carbon–PTFE air-diffusion cathode. The aim was to check the feasibility of operating at circumneutral pH (5.5–7.4) with the employment of low amounts of carboxylate ligand and iron. To the best of our knowledge, this is the first time that a PEF process mediated by Fe(III)–carboxylate complexes is studied and its efficiency assessed considering the different iron complexes present in solution and the photoactivity of each ferric species. Carboxylate ligands like oxalate, citrate, tartrate and malate were investigated and the influence of Fe(III)-to-carboxylate molar ratio and pH was also assessed. In addition, the effect of initial TMP concentration and temperature was considered and the role of the different reactive oxidizing species on the degradation processes was clarified by adding scavenging agents. Generated carboxylic acids were followed throughout reactions by ion-exclusion HPLC.

2. Experimental

2.1. Chemicals

Trimethoprim ($C_{14}H_{18}N_4O_3$, ≥99.0%) was of HPLC grade purchased from Sigma-Aldrich. Sodium sulfate anhydrous, used as background electrolyte, and iron(III) chloride hexahydrate, used as catalyst, were of analytical grade purchased from Merck. Oxalic acid dihydrate, citric acid monohydrate, tartaric acid and L(−)-malic acid, used as ligands, were of analytical grade supplied by VWR-Prolabo (the first two), Sigma-Aldrich and Acros Organics, respectively. Concentrated sulfuric acid and sodium hydroxide, both of analytical grade and used for pH adjustment, were supplied by Pronalab and Merck, respectively. D-Mannitol (ACS reagent) and sodium azide (analytical grade), used as scavenging agents, were purchased from Sigma-Aldrich and Panreac, respectively. All the other chemicals were either of HPLC grade or analytical grade supplied by VWR-Prolabo, Sigma-Aldrich, Panreac, Merck, Fisher Chemical and Pronalab. All the solutions were prepared with ultrapure water produced by a Millipore® Direct-Q system (18.2 MΩ cm resistivity at 25 °C).

2.2. Experimental system

Electrochemical experiments were performed in a 2.2 L lab-scale flow plant composed of: (i) a thermostatically controlled 1.5 L capacity cylindrical glass vessel, (ii) a photo reactor with a double CPC of 694 mL irradiated volume and (iii) an electrochemical filter-press MicroFlowCell reactor with a 10 cm^2 BDD anode and a 10 cm^2 carbon-PTFE air-diffusion cathode. A detailed description of the characteristics of these components has been previously provided in Moreira et al. [39].

2.3. Experimental procedure

The temperature controller was switched on at a temperature set-point that permitted to preserve the solution at 10, 20 or 40 °C.

A volume of 1.340 L of a solution composed of 6.9, 17.2, 34.4 and 68.9 μM TMP and 50 mM Na_2SO_4 was added to the glass vessel and homogenized by recirculation during 10 min in darkness and a 30 mL first control sample was taken for further characterization (irradiated volume/total volume ratio of 0.52; irradiated time of 1.04 min; dark time of 0.97 min). Solutions with Fe(III)–carboxylate complexes were prepared by directly mixing aqueous solutions of the carboxylic acid (oxalic, citric, tartaric or malic acid) and $FeCl_3{\cdot}6H_2O$ at a chosen Fe(III)-to-ligand molar ratio (1:1, 1:3, 1:6 or 1:9). To do this, each carboxylic acid was added to the solution at a selected dose and the solution was homogenized during 10 min in the darkness (a 30 mL second sample was taken). Afterwards, the $FeCl_3{\cdot}7H_2O$ (35.8 μM Fe^{3+}) was added and, after solution homogenization for another 10 min in the dark, the pH was adjusted to a desired value and a final mixing for another 10 min in dark took place (a 30 mL third sample was taken). Addition of scavenging agents was performed before pH adjustment and was followed by a 10 min homogenization in darkness. Finally, j was set at 5 mA cm^{-2} and at the same time the UVA lamp was switched on. Samples of 30 mL were taken at different time intervals to evaluate the degradation process, which included: (i) TMP concentration decay; (ii) total dissolved organic carbon (DOC) abatement; (iii) H_2O_2 concentration; (iv) dissolved iron concentration (Fe^{2+}, Fe^{3+} and total dissolved iron) and (v) pH. To remove impurities of the BDD surface and activate the cathode, the electrodes were previously polarized in 50 mM Na_2SO_4 at 100 mA cm^{-2} for 180 min.

2.4. Analytical measurements

Before analysis, all the samples were filtered with 0.45 μm Nylon filters purchased from Whatman. The analytical procedures on TMP concentration measurement and the detection of generated carboxylic acids were reported elsewhere [39]. Before all HPLC analysis, 1 M methanol, a well-known •OH scavenger ($k_{•OH} = 9.7 \times 10^8$ $(M\,s)^{-1}$) [29], was added to the samples in order to stop the mineralization process. DOC concentration was directly determined on a Shimadzu TOC-VCSN analyzer equipped with an ASI-V auto sampler. Na_2SO_3 in a Na_2SO_3-to-H_2O_2 molar ratio of 1:1 [40] was alternatively added to the DOC samples in order to quench H_2O_2 and stop the mineralization process. H_2O_2 concentration was measured by the colorimetric metavanadate method [41]. Fe^{2+}, Fe^{3+} and total dissolved iron concentrations were determined according to the colorimetric 1,10-phenantroline standardized procedure [42]. UV–vis measurements were performed with a VWR UV-6300PC spectrophotometer.

2.5. Model parameters estimation

A pseudo-first-order kinetic model was fitted to the experimental data as a simple mathematical model from which properly kinetic constants could be calculate to quantitatively compare the various reactions under distinct conditions. This kinetic model was adjusted by a nonlinear regression method using the Fig. P software for Windows from Biosoft. The pseudo-first-order kinetic constants for TMP concentration decay (k_{TMP}) and DOC removal (k_{DOC}), both in min^{-1}, were calculated as follows:

$$[TMP]_t = [TMP]_0 \times e^{-k_{TMP} \times t} \quad (7)$$

$$[DOC]_t = [DOC]_0 \times e^{-k_{DOC} \times t} \quad (8)$$

where the subscripts 0 and t denote the TMP or DOC concentrations when reaction starts and after t time, respectively. The initial TMP and DOC removal rates ($r_{0(TMP)}$ and $r_{0(DOC)}$), in μM min^{-1}, were obtained from Eqs. (9) and (10), respectively:

$$r_{0(TMP)} = k_{TMP} \times [TMP]_0 \quad (9)$$

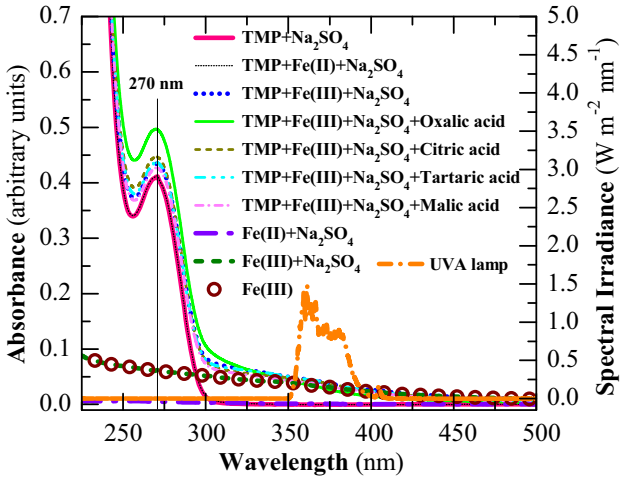

Fig. 1. Absorption spectra of different solutions at pH = 3.5. [TMP] = 68.9 μM, [Na_2SO_4] = 50 mM, [Fe^{2+}] = 35.8 μM, [Fe^{3+}] = 35.8 μM, 1:3 Fe(III)-to-oxalate molar ratio, 1:1 Fe(III)-to-citrate molar ratio, 1:1 Fe(III)-to-tartrate molar ratio and 1:1 Fe(III)-to-malate molar ratio. The spectral irradiance of the UVA lamp is also shown.

$$r_{0(DOC)} = k_{DOC} \times [DOC]_0 \quad (10)$$

The resulting kinetics parameters were found by minimizing the sum of the squared deviations between experimental and predicted values. The goodness of all these parameters was assessed by calculating the relative standard deviations, the coefficient of determination (R^2) and the residual variance (S^2_R).

3. Results and discussion

3.1. UV–vis spectra of different solutions

Fig. 1 illustrates the absorption spectra of various solutions at pH 3.5. Note that this pH was selected in order to minimize iron precipitation, as can be seen in the Fe^{3+} speciation diagrams including $Fe(OH)_{3(s)}$ formation in Figs. SM-1b and d of Supplementary material and Fig. 2. The Fe^{3+} solution displayed an absorption in the range of 200–500 nm that can be attributed to the formation of Fe(III)–hydroxy complexes such as $FeOH^{2+}$ and mainly $Fe(OH)_2^+$, which are the predominant species in this system according to the calculated Fe^{3+} speciation diagrams (see Figs. SM-1c and d). The addition of Na_2SO_4 to this solution did not affect its ability to absorb radiation due to the presence of quite similar amounts of $FeOH^{2+}$ and $Fe(OH)_2^+$, despite of the availability of Fe(III)–sulfate complexes like $FeSO_4^+$ and $Fe(SO_4)_2^-$ (see Fig. SM-1). The TMP antibiotic solution exhibited a maximum absorption at 270 nm and after the addition of Fe^{3+} the absorbance raised in all the wavelength range, principally for values above 300 nm, which can be linked to the formation of Fe(III)–hydroxy complexes. No evidence of Fe(III)–TMP complexes [43,44] formation was found by spectra analysis. In the presence of Fe^{2+} at pH 3.5, the formation of Fe(II)–hydroxy complexes is not expected from the Fe^{2+} speciation diagram (data not displayed) and there is no evidence of Fe(II)–TMP species formation. The establishment of $FeSO_4$, the only Fe(II)–sulfate complex that is expected to be present under the current conditions, revealed to have a negligible influence on the solution absorbance. On the other hand, the absorbance of the solutions containing Fe(III)/TMP/oxalate, Fe(III)/TMP/citrate and Fe(III)/TMP/tartrate was higher than that of the Fe(III)/TMP solutions for wavelengths between 240 and 325 nm, especially in the former case. In contrast, the presence of Fe(III)–malate complexes did not increase the absorbance.

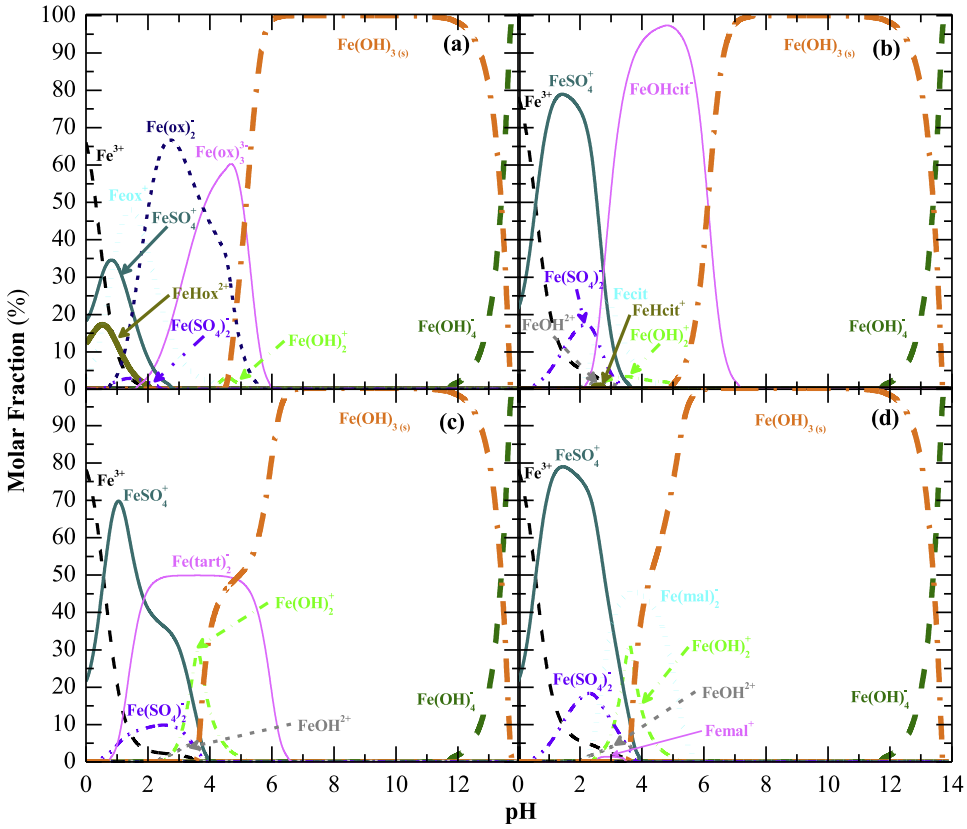

Fig. 2. Theoretical Fe^{3+} speciation diagrams as a function of the solution pH in a system containing (a) 107 μM oxalate ion (1:3 Fe(III)-to-oxalate molar ratio), (b) 35.8 μM citrate ion (1:1 Fe(III)-to-citrate molar ratio), (c) 35.8 μM tartrate ion (1:1 Fe(III)-to-tartrate molar ratio) or (d) 35.8 μM malate ion (1:1 Fe(III)-to-malate molar ratio), with 35.8 μM Fe^{3+}, 49.3 mM SO_4^{2-}, 98.6 mM Na^+ and 107 μM Cl^- (ionic strength = 148 mM). Data were calculated from the chemical equilibrium modeling system MINEQL+ [52], using the equilibrium constants of Table SM-1 of Supplementary material. The formation of the solid iron phase $Fe(OH)_3$ was included in the calculation despite of the slow formation of solid phases on the time scale of the experiments.

3.2. Preliminary results for TMP degradation

The TMP concentration of 68.9 μM (20.0 mg L^{-1}) was much higher than that found in aquatic systems (ng L^{-1} or μg L^{-1} levels) in order to attain comprehensive TMP and DOC decay profiles to explain the degradation behavior. This antibiotic content corresponds to a DOC of 11.6 mg L^{-1} and a chemical oxygen demand (COD) of 704 g O_2 per mol TMP.

Moreira et al. [39] performed a detailed study on the treatment of 68.9 μM TMP in 50 mM Na_2SO_4 by PEF using the lab-scale flow plant at a flow rate of 40 L h^{-1} and 20 °C (an ambient temperature largely found in WWTPs final effluents [45]). This process revealed effectiveness using a low iron concentration of 35.8 μM (2.0 mg L^{-1}), which is the Portuguese total iron discharge limit for WWTPs final effluents (Portuguese decree law no. 236/98), avoiding the need for iron removal. Operating at a low current density of 5 mA cm^{-2}, a maximum suitable pH of 3.5 without iron precipitation was found, suggesting the necessity of the use of Fe(III)–carboxylate complexes to rise the working pH to circumneutral values.

A PEF experiment of the above antibiotic solution was then performed under the reported conditions but using pH 5.0 in the presence of 1:3 Fe(III)-to-oxalate molar ratio without pH regulation. A continuous rise in pH was observed up to reach a value of 6.4 after 180 min of electrolysis, which can be attributed to oxalic acid degradation and compromises the data interpretation. As a result, further trials were accomplished with pH adjustment to the initial value during the entire electrolysis time by adding small amounts of 0.5 M H_2SO_4. Note that in all the PEF trials performed, the H_2O_2 generated from Eq. (3) was continuously accumulated in the solution from 118–206 μM to 1029–1588 μM after 30 and 180 min, respectively (data not shown). This excess in H_2O_2 production ensures the maximum •OH production in the solution bulk from Fenton's reaction (2).

3.3. PEF degradation in the presence of various Fe(III)–carboxylate complexes

The influence of the nature of the carboxylate ligand on TMP degradation by PEF in the lab-scale flow plant was assessed by degrading 1.340 L of 68.9 μM TMP solutions in 50 mM Na_2SO_4 with 35.8 μM Fe^{3+} at pH 4.5, 20 °C, 5 mA cm^{-2} and flow rate of 40 L h^{-1}. The stoichiometry of Fe(III)-to-carboxylate complexes was 1:3 for Fe(III)–oxalate and 1:1 for Fe(III)–citrate, Fe(III)–tartrate and Fe(III)–malate complexes, which has been reported as optimal by several authors [19,46–49]. Figs. 3a and b depict quite similar TMP and DOC decays for the PEF treatments with the three first Fe(III)–carboxylate complexes, contrasting with the treatment with the Fe(III)–malate system, which displayed inferior ability to remove both TMP and DOC contents, with k_{TMP} and k_{DOC} values 1.5–2.3 and 2.2–2.5 times smaller (see Tables 1 and 2), respectively. All the systems underwent a low DOC abatement that can be mainly attributed to the formation of high amounts of nitrogenated by-products, even more recalcitrant than TMP parent compound, as reported in other studies [39,50,51]. The low ability of PEF to degrade intermediates cannot be related to the influence of sulfate ions present in the background electrolyte since: (i) according to Fe^{3+} speciation diagrams at pH 4.5, the formation of Fe(III)–sulfate complexes has almost negligible effects on the distribution of Fe(III)–carboxylate and Fe(III)–hydroxy complexes either in the

Table 1
Pseudo-first-order kinetic constants for TMP concentration decay (k_{TMP}) and initial TMP removal rates ($r_{0(TMP)}$), along with the corresponding coefficient of determination (R^2) and residual variance (S^2_R), obtained for the PEF degradation of TMP solutions under the conditions of Figs. 2, 5–7 and 9.

System	pH	Fe(III):L	k_{TMP} ($\times10^{-2}$ min^{-1})	$r_{0(TMP)}$ ($\times10^{-2}$ μM min^{-1})	R^2	S^2_R (μM^2)
PEF	3.5	–	2.4 ± 0.1	163 ± 3	0.997	0.73
PEF with Fe(III)–oxalate	4.5	1:3	4.8 ± 0.1	280 ± 6	0.999	1.03
PEF with Fe(III)–citrate	4.5	1:1	6.1 ± 0.2	264 ± 10	0.998	1.16
PEF with Fe(III)–tartrate	4.5	1:1	3.9 ± 0.1	218 ± 7	0.996	2.28
PEF with Fe(III)–malate	4.5	1:1	2.7 ± 0.1	154 ± 3	0.998	1.34
PEF with Fe(III)–oxalate	4.5	1:3	4.8 ± 0.1	280 ± 6	0.999	1.03
	5.0	1:3	2.28 ± 0.04	151 ± 3	0.998	1.58
	5.0	1:6	4.6 ± 0.2	315 ± 10	0.996	4.01
PEF with Fe(III)–citrate	5.0	1:9	7.4 ± 0.2	230 ± 6	0.999	0.30
	5.5	1:9	4.1 ± 0.1	281 ± 7	0.998	2.65
	5.0	1:1	2.8 ± 0.1	154 ± 4	0.996	1.40
		Parameter				
TMP concentration (mg L^{-1})	2.0		18.9 ± 0.8	113 ± 5	0.995	0.05
	5.0		11.4 ± 0.8	161 ± 12	0.987	0.43
	10.0		8.0 ± 0.4	227 ± 11	0.996	0.70
	20.0		6.1 ± 0.2	264 ± 10	0.998	1.16
Temperature (°C)	10		4.4 ± 0.3	278 ± 16	0.992	8.77
	20		4.8 ± 0.1	280 ± 6	0.999	1.03
	40		8.1 ± 0.2	454 ± 11	0.998	0.88
Scavenging agents	Absence		6.1 ± 0.2	264 ± 10	0.998	1.16
	D-Mannitol		0.64 ± 0.01	43 ± 1	0.998	0.64
	Sodium azide		0.37 ± 0.01	24 ± 1	0.984	1.52

presence of oxalic, citric, tartaric and malic acids (see Fig. 2 (with sulfate) and Fig. SM-2 of Supplementary material (without sulfate)) and in their absence (see Fig. SM-1 (with and without sulfate)); and (ii) no hydrogensulfate ions are available at pH 4.5 according to SO_4^{2-} speciation diagram (data not displayed) and then no $^{\bullet}OH$ scavenging together with the formation of the less reactive sulfate anion radical ($SO_4^{\bullet-}$) from Eq. (11) may occur [28].

$$HSO_4^- + {}^{\bullet}OH \rightarrow SO_4^{\bullet-} + H_2O \quad (11)$$

Figs. 3a and b also revealed that the PEF processes mediated by Fe(III)–carboxylate complexes at pH 4.5 yielded faster TMP and DOC abatements than the classical PEF one (absence of the initial supply of a carboxylic acid) at pH 3.5, with k_{TMP} and k_{DOC} values 1.1–2.5 and 1.7–2.0 times higher (see Tables 1 and 2), respectively, except for the DOC decay of the Fe(III)–malate system. The greater oxidation ability of PEF in the presence of Fe(III)–carboxylate complexes can be mainly associated with: (i) the superiority of quantum yields of Fe^{2+} formation from the Fe(III)–carboxylate complexes over Fe(III)–hydroxy complexes [22,30,31], because of the greater absorption of UVA light as confirmed from absorption spectra of Fig. 1; and (ii) a possible prevention of the formation of Fe(III)–TMP complexes [25,33–35] or other Fe(III)–organic complexes with low photoactivity, with the consequent improvement of Fe^{3+} regeneration to Fe^{2+} and hence the overall efficiency of the PEF process.

Rodríguez et al. [31] determined the efficiencies of Fe(III)–carboxylate complexes to degrade 50 μM muconic acid solutions with 50 μM Fe^{3+} at pH 3.0 and 20 °C using Fe(III)-to-carboxylate molar ratios of 1:2 and 15 W black light lamps

Table 2
Pseudo-first-order kinetic constants for DOC removal(k_{DOC}) and initial DOC removal rates ($r_{0(DOC)}$), along with the corresponding coefficient of determination (R^2) and residual variance (S^2_R), obtained for the PEF treatment of TMP solutions under the conditions of Figs. 2, 5–7.

System	pH	Fe(III):L	Period	k_{DOC} ($\times10^{-3}$ min^{-1})	$r_{0(DOC)}$ ($\times10^{-3}$ mg L^{-1} min^{-1})	R^2	S^2_R (mg^2 L^{-2})
PEF	3.5	–	–	2.1 ± 0.1	24.5 ± 0.6	0.995	0.010
PEF with Fe(III)–oxalate	4.5	1:3	–	3.5 ± 0.2	39 ± 2	0.978	0.066
PEF with Fe(III)–citrate	4.5	1:1	–	4.2 ± 0.1	58 ± 1	0.997	0.015
PEF with Fe(III)–tartrate	4.5	1:1	–	3.8 ± 0.1	52 ± 2	0.992	0.033
PEF with Fe(III)–malate	4.5	1:1	–	1.6 ± 0.1	22 ± 1	0.966	0.052
	4.5	1:3	–	3.5 ± 0.2	39 ± 2	0.978	0.066
	5.0	1:3	–	3.5 ± 0.1	50 ± 2	0.993	0.027
	5.0	1:6	1st	7.5 ± 0.4	131 ± 8	0.989	0.120
PEF with Fe(III)–oxalate			2nd	0.5 ± 0.1	5 ± 2	0.943	0.104
	5.0	1:9	1st	9.0 ± 0.2	180 ± 4	0.998	0.057
			2nd	0.6 ± 0.2	6 ± 2	0.997	0.205
	5.5	1:9	1st	7.5 ± 0.2	156 ± 4	0.997	0.066
			2nd	0.6 ± 0.1	6 ± 2	0.995	0.168
PEF with Fe(III)–citrate	5.0	1:1	–	2.73 ± 0.04	38.2 ± 0.6	0.996	0.014
		Parameter					
TMP concentration (mg L^{-1})	2.0		–	6.2 ± 0.1	15.2 ± 0.1	1.000	0.0001
	5.0		–	6.2 ± 0.1	21.4 ± 0.3	0.999	0.001
	10.0		–	6.3 ± 0.1	56 ± 1	0.998	0.006
	20.0		–	4.2 ± 0.1	58 ± 1	0.997	0.015
Temperature (°C)	10		–	3.9 ± 0.3	46 ± 3	0.971	0.115
	20		–	3.5 ± 0.2	39 ± 2	0.978	0.066
	40		1st	8.8 ± 0.8	127 ± 9	0.972	0.257
			2nd	2.6 ± 0.1	22.8 ± 0.9	0.989	0.008

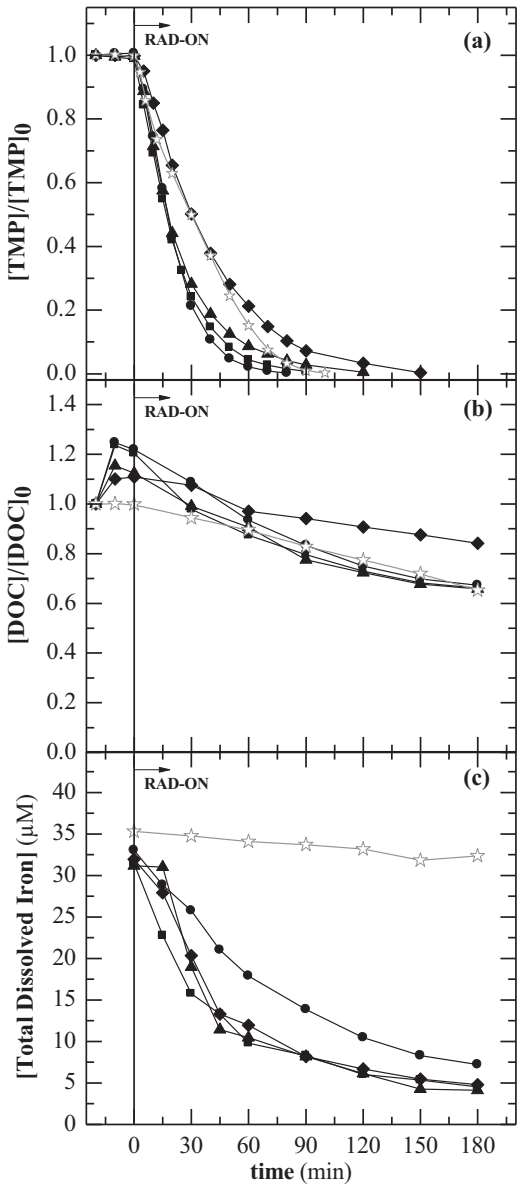

Fig. 3. Effect of Fe(III)–carboxylate complexes on (a) normalized TMP concentration decay, (b) normalized DOC removal and (c) total dissolved iron concentration as a function of time for the PEF degradation in the lab-scale flow plant of a 68.9 μM TMP solution in 50 mM Na_2SO_4 with $[Fe^{3+}]_0$ = 35.8 μM at pH = 4.5, j = 5 mA cm^{-2}, 20 °C and flow rate of 40 L h^{-1}. Fe(III)–carboxylate complex (Fe(III)-to-carboxylate molar ratio): (■) Fe(III)–oxalate (1:3), (●) Fe(III)–citrate (1:1), (▲), Fe(III)–tartrate (1:1) and (♦) Fe(III)–malate (1:1). (☆) Classical PEF process (only with Fe^{3+}) at pH 3.5.

emitting between 350 and 400 nm with λ_{max} = 365 nm. They found the following performance: Fe(III)–oxalate > Fe(III)–citrate ≈ Fe(III)–tartrate > Fe(III)–malate, with quantum yields of 0.993, 0.589, 1.102 and 0.510 mol per photon, in terms of Fe^{2+} formation, respectively. Abrahamson et al. [30] reported decreasing quantum yields in the order Fe(III)–tartrate (0.58) > Fe(III)–citrate (0.45) > Fe(III)–oxalate (0.30) > Fe(III)–malate (0.29) at pH 4.0 and Fe(III)–oxalate (0.65) > Fe(III)–tartrate (0.40) > Fe(III)–citrate (0.28) > Fe(III)–malate (0.21) at pH 2.7, both using 300 μM Fe^{3+}, Fe(III)-to-carboxylate molar ratio of 1:5 and a broad-band UV irradiation. The superiority of Fe(III)–oxalate, Fe(III)–citrate and Fe(III)–tartrate over Fe(III)–malate complexes was always patent in both reported works, in agreement with the results obtained in this study. However, the above quantum yield values were determined under different experimental conditions like initial Fe(III)-to-carboxylate ratio, wavelength of the light source and pH and thus they should be taken carefully since these variables can affect them in different extent.

To clarify in detail the type of Fe(III)–carboxylate species acting in each PEF system and their proportion, Fe^{3+} speciation diagrams were calculated by the chemical equilibrium modeling system MINEQL+ [52] as a function of the solution pH considering the initial experimental conditions, as can be seen in Fig. 2. The Fe^{3+} speciation diagram of the Fe(III)–oxalate system in Fig. 2a shows the presence of four Fe(III)–oxalate complexes, $FeHox^{2+}$, $Feox^{+}$, $Fe(ox)_2^{-}$ and $Fe(ox)_3^{3-}$. $FeHox^{2+}$ species acts at pH values below 2.1 in molar fractions lower than 18%, whereas $Feox^{+}$ is available at a maximum molar fraction of 48% at pH 1.4 and from this point its amount is decreasing up to disappear at pH 4.5. From pH 2.0 to 5.1, the predominant Fe(III)–oxalate complexes are the most photoactive $Fe(ox)_2^{-}$ and $Fe(ox)_3^{3-}$ species [19], which account for a total molar fraction of 95–97% at pH 3.4–4.5, thereby covering the pH of 4.5 used in the PEF treatment. As a result, the high TMP degradation by this process shown in Fig. 3a confirms the high photoactivity of $Fe(ox)_2^{-}$ and $Fe(ox)_3^{3-}$. The Fe(III)–citrate speciation diagram (Fig. 2b) reveals the existence of three Fe(III)–citrate species, $FeOHcit^{-}$, Fecit and $FeHcit^{+}$, within the pH range from 2.0 to 7.1. $FeOHcit^{-}$ is the dominant species at a pH range of 3.0–6.1 with maximum molar fractions of 95–97% at pH 4.2–5.2. The great TMP degradation reached using the PEF system with Fe(III)–citrate complexes (see Fig. 3a) suggests a high quantum yield of the $FeOHcit^{-}$ species for Fe^{2+} formation. In turn, the equilibrium speciation of Fe(III)–tartrate system given in Fig. 2c indicates the occurrence of a single $Fe(tart)_2^{-}$ species available from pH 0.8 to 6.5, with a highest molar fraction of 47–50% at pH 2.1–5.2. Since PEF with Fe(III)–tartrate complexes also underwent a high TMP degradation (Fig. 3a), it is highly likely that $Fe(tart)_2^{-}$ species owns high photoactivity. Finally, Fig. 2d displays the attendance of two Fe(III)–malate complexes, $Femal^{+}$ and $Fe(mal)_2^{-}$, although the former presents very low molar fractions (<1.5%) and the maximum $Fe(mal)_2^{-}$ molar fraction of 43–46% occurs from pH 3.3 to 4.2, whereas at pH 4.5 this species is available in 40%. Note that in PEF systems with Fe(III)–citrate, Fe(III)–tartrate and Fe(III)–malate complexes, the $FeOH^{2+}$ species is also available but in amounts lower than 5.2% at pH values lesser than 4.0, not affecting the oxidation ability of the PEF processes performed at pH 4.5.

Beyond the influence of quantum yields for Fe^{2+} formation on TMP degradation efficiency, the rate of photodecarboxylation of Fe(III)–carboxylate complexes can also affect the process since their presence allows preserving dissolved iron in solution with the consequent enhancement of TMP removal. Several authors have reported half-life of few minutes for Fe(III)–carboxylate complexes under UVA radiation [19,22,53]. This was confirmed by analyzing the treated TMP solutions by ion-exclusion HPLC. Figs. 4b–d reveal a rapid and total degradation of citric, tartaric and malic acids after less than 10–15 min of electrolysis. In contrast, Fig. 4a shows that oxalic acid sharply declined during the first 40 min, further remaining in solution at concentrations around 7.9 μM, due to the continuous formation of this acid as by-product of TMP degradation. Since Fe(III)–carboxylate complexes are quickly photodecarboxylated, their Fe^{3+} speciation diagrams in the initial conditions are inappropriate to describe properly their photocatalytic action during the entire reaction time. However, the construction of Fe^{3+} speciation diagrams with different doses of carboxylic acids showed that their degradation yielded lower amounts of Fe(III)–carboxylate species along with the precipitation of iron as $Fe(OH)_{3(s)}$ at progressively inferior pH values (data not shown).

The theoretical ability of Fe^{3+} to precipitate at initial conditions was checked by including the $Fe(OH)_{3(s)}$ formation in the calculation of speciation diagrams. At pH 4.5, the corresponding

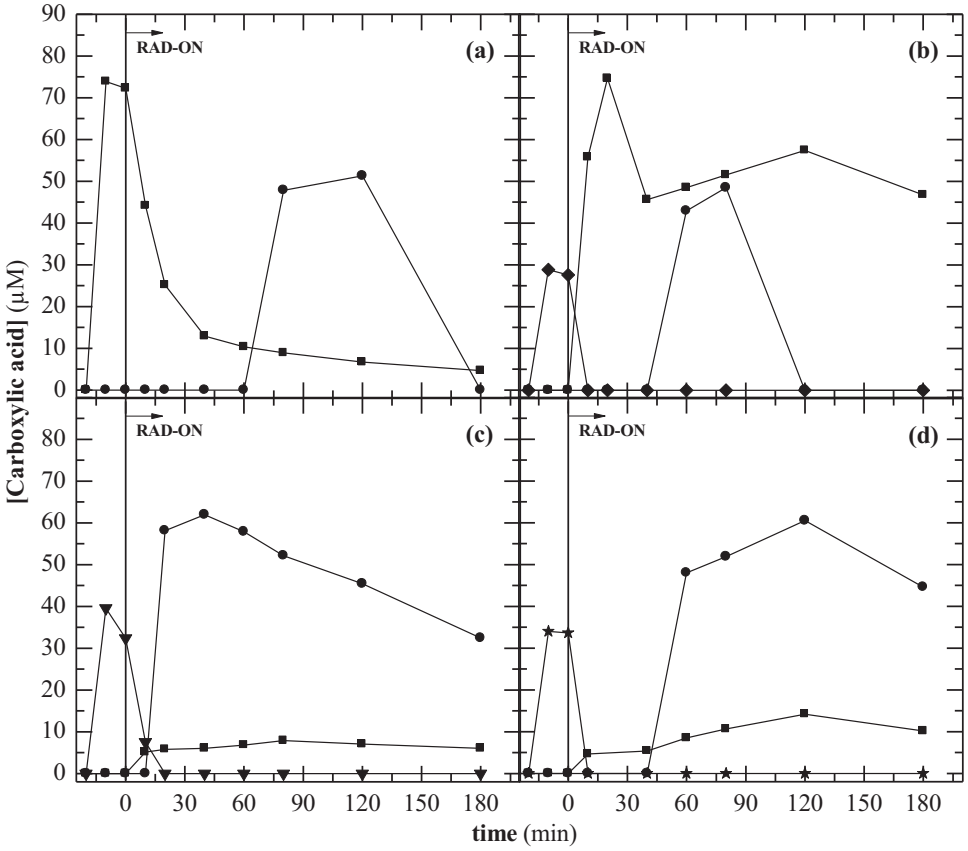

Fig. 4. Evolution of the concentration of (■) oxalic, (●) formic, (♦) citric, (▼) tartaric and (⋆) malic acids during the PEF degradations under the conditions of Fig. 2. System: (a) Fe(III)–oxalate, (b) Fe(III)–citrate, (c) Fe(III)–tartrate and (d) Fe(III)–malate.

diagrams of Fig. 2 predict null Fe^{3+} precipitation in Fe(III)–oxalate and Fe(III)–citrate systems, whereas molar fractions of 46% and 56% for $Fe(OH)_{3(s)}$ were formed in the Fe(III)–tartrate and Fe(III)–malate systems, respectively. However, the fast photodecarboxylation of all carboxylic acids led to the achievement of quite similar profiles of total dissolved iron using the Fe(III)–oxalate, Fe(III)–tartrate and Fe(III)–malate systems, decreasing to values below 17.9 μM Fe after approximately 30 min of reaction, as can be seen in Fig. 3c. Nevertheless, the Fe(III)–citrate system exhibited higher values of total dissolved iron along all the electrolysis time, above 17.9 μM until ca. 60 min. Regarding the generated short-chain carboxylic acids in Fig. 4, oxalic acid was found in 46–75 μM in the Fe(III)–citrate system whereas lower amounts, below 15 μM, were accumulated in the other systems. Consequently, a greater Fe^{3+} content can be available in the form of Fe(III)–oxalate complexes using the Fe(III)–citrate system in PEF, thereby justifying the inferior iron precipitation attained on it. Note that the $Fe(OH)_{3(s)}$ phase was formed very slowly, which can explain its absence at the starting time in Fe(III)–tartrate and Fe(III)–malate systems despite of their prevision from their speciation diagrams. A total dissolved iron concentration of around 17.9 μM then proved that can be efficiently used for the degradation of TMP using PEF process. In the presence of lower amounts of iron or in its absence, TMP and its intermediates may be pre-eminently degraded by BDD(•OH), thus explaining the slow TMP and DOC removal found for the PEF processes at longer electrolysis times.

Apart oxalic acid, oxamic and formic acids were also detected during all PEF processes with Fe(III)–carboxylate complexes. All these acids are ultimate carboxylic acids since they are directly mineralized to CO_2 [54,55]. Oxamic acid was always found at contents lower than 0.5 μM. Formic acid exhibited higher molar concentrations than the other acids up to 62 μM. After 180 min of PEF treatment, only 2–15% of remaining DOC was due to generated carboxylic acids.

3.4. Influence of pH and initial Fe(III)-to-carboxylate molar ratio

The effects of pH and initial Fe(III)-to-carboxylate molar ratio were evaluated in the PEF treatments mediated by Fe(III)–oxalate and Fe(III)–citrate complexes using pH values from 4.5 to 5.5 and Fe(III)-to-carboxylate molar ratios of 1:3, 1:6 and 1:9 in the former system and pH values of 4.5 and 5.0 and a 1:1 molar ratio in the latter one.

Fig. 5a discloses similar TMP decay profiles at pH 4.5, 5.0 and 5.5 for Fe(III)-to-oxalate molar ratios of 1:3, 1:6 and 1:9 respectively, with complete disappearance of TMP in 90 min in all cases. This advises to the need of using double and triple oxalate ligand molar concentration to obtain similar results at pH 5.0 and 5.5, respectively, when compared to pH 4.5. Fe^{3+} speciation diagrams (see diagrams of 1:6 and 1:9 Fe(III)-to-oxalate molar ratios in Fig. SM-3 of Supplementary material) showed a similar molar fractions of 95–100% for the sum of $Fe(ox)_2^-$ and $Fe(ox)_3^{3-}$ species and no iron precipitation under the three preceding conditions, supporting the achieved findings. The use at pH 5.0 of a Fe(III)-to-oxalate molar ratio of 1:3 against 1:6 led to a slower TMP removal with a k_{TMP} value 2.0 times inferior (see Table 1) and complete disappearance after only 180 min, which can be mainly linked to: (i) a higher iron precipitation since the use of a 1:3 Fe(III)-to-oxalate molar ratio estimates the presence of a $Fe(OH)_{3(s)}$ molar fraction of 34% at initial conditions (see Fig. 2a) and (ii) the availability of lower amounts of Fe(III)–oxalate complexes, disappearing from the solution at shorter reaction times. In fact, the total dissolved iron

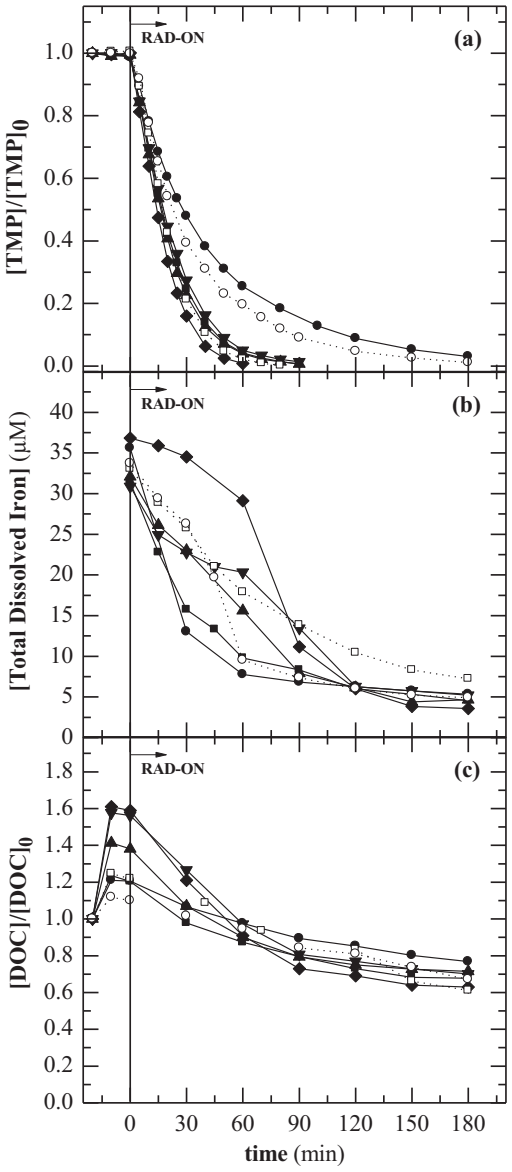

Fig. 5. Effect of pH and initial Fe(III)-to-carboxylate molar ratio on (a) normalized TMP concentration decay, (b) total dissolved iron concentration and (c) normalized DOC removal as a function of time for the PEF degradation in the lab-scale flow plant of a 68.9 μM TMP solution in 50 mM Na_2SO_4 with 35.8 μM Fe^{3+} at j = 5 mA cm^{-2}, 20 °C and flow rate of 40 L h^{-1}. Conditions: (■) pH = 4.5 and 1:3 Fe(III)-to-oxalate molar ratio, (●) pH = 5.0 and 1:3 Fe(III)-to-oxalate molar ratio, (▲) pH = 5.0 and 1:6 Fe(III)-to-oxalate molar ratio, (♦) pH = 5.0 and 1:9 Fe(III)-to-oxalate molar ratio, (▼) pH = 5.5 and 1:9 Fe(III)-to-oxalate molar ratio, (□) pH = 4.5 and 1:1 Fe(III)-to-citrate molar ratio and (○) pH = 5.0 and 1:1 Fe(III)-to-citrate molar ratio.

attained a value below 17.9 μM after ca. 25 min of treatment (see Fig. 5b) when only 47% of TMP had been removed. On the other hand, the use at pH 5.0 of a Fe(III)-to-oxalate molar ratio of 1:9 in contrast to 1:6 had an increase on TMP degradation with k_{TMP} 1.6 times higher (see Table 1), because iron remained in solution in much higher concentrations during longer times of ca. 90 min.

When 1:6 and 1:9 Fe(III)-to-oxalate molar ratios were employed, the DOC decay profiles of Fig. 5c were characterized by an initial period with sharp declines and a second period with a very slowly decay, probably due to the formation of nitrogenated organic oxidation products hardly oxidized by BDD(•OH), •OH in the bulk and/or photo decomposed by UVA light as stated above. A Fe(III)-to-oxalate molar ratio of 1:9 compared to 1:6 led to a larger initial period of 90 against 60 min with more pronounced DOC removal, giving slightly higher $r_{0(DOC)}$ values (see Table 2). In contrast, the DOC profiles of the systems employing a 1:3 Fe(III)-to-oxalate molar ratio, as well as the aforementioned systems with a 1:1 Fe(III)-to-carboxylate molar ratio, did not experienced an initial quicker DOC abatement. These findings suggest that during this initial phase occurred the mineralization of oxalic acid since when changing from Fe(III)-to-oxalate molar fraction of 1:9 to 1:3 this acid gradually contributes less to DOC content (addition of 7.7, 5.2 and 2.6 mg C L^{-1} for molar ratios of 1:9, 1:6 and 1:3, respectively).

The increment of pH value from 4.5 to 5.0 in the Fe(III)–citrate system led to slower TMP and DOC decays (see Figs. 5a and c), with k_{TMP} and k_{DOC} values 2.1 and 1.5 times inferior, respectively (see Tables 1 and 2), along with faster decrease of total dissolved iron (see Fig. 5b). The analysis of the evolution of short-chain carboxylic acids showed a fast citric acid degradation in both systems and the formation of 6.3–15 μM of oxalic acid at pH 5.0 (data not displayed), values inferior to 46–75 μM accumulated at the pH 4.5 system. The presence of smaller amounts of Fe(III)–oxalate complexes in the Fe(III)–citrate system at pH 5.0 then corroborates the faster decay of total dissolved iron, leading to a low process efficiency.

Despite of the better results achieved when higher Fe(III)-to-carboxylate molar fractions were applied, the use of high carboxylic acids should be taken with precaution not only because of the presence of an excess of carboxylate ions that cannot be complexed with the Fe^{3+} ions present in solution and can act as extra carbon source, but also due to a decrease of light penetration throughout the solution and the necessity to support higher reagent costs.

3.5. Effect of initial TMP concentration

The influence of initial TMP concentration, 2.0, 5.0, 10.0 and 20.0 mg L^{-1} (6.9, 17.2, 34.4 and 68.9 μM), on the PEF process was assessed at pH 4.5 in the presence of 1:1 Fe(III)-to-citrate molar ratio under the abovementioned conditions. Fig. 6a reveals raising TMP removal rates for greater initial TMP concentration, with $r_{0(TMP)}$ values 1.4, 2.0 and 2.3 times higher for 17.2, 34.4 and 68.9 μM compared to 6.9 μM, respectively (see Table 1), leading to the removal of higher amounts of the antibiotic per unit of time. In view of the pseudo-first-order kinetic model, it should be expected an independence of k_{TMP} on the organic content, which is in disagreement with the detected large drop of this parameter when TMP concentration rises (see Table 1). Hence, the pseudo-first-order kinetic model may comprise some limitations to describe precisely the TMP decay profiles, as predictable since a comprehensive mechanistic kinetic model may include all chemical, photocatalytic and electrochemical reactions that each contaminant (TMP, carboxylic acids and all intermediates formed) undergoes in the treatment. Furthermore, lower diffusion of H_2O_2 and Fe^{2+} species and mass transport toward/from electrodes can be achieved in the presence of higher substrate concentration (organic matter content), thus diminishing the •OH production, as proposed by El-Ghenymy et al. [6]. Conversely, Fig. 6b shows similar kinetics for DOC removal, with quite analogous k_{DOC} values for all tested antibiotic contents and gradual increase of $r_{0(TMP)}$ with TMP concentration raise (see Table 2). The normalized DOC abatement profiles of the two lowest 2.0 and 5.0 mg L^{-1} TMP solutions layout an initial phase characterized by a more pronounced decay and a subsequent period with slow decline. The initial fast period can be related to the degradation of Fe(III)–citrate complexes since lower TMP doses resulted in a higher ratio between the DOC of citric acid (2.6 mg C L^{-1} in all the trials) and the antibiotic (11.6, 5.8, 2.9 and 1.2 mg C L^{-1} for 6.9, 17.2, 34.4 and 68.9 μM TMP, respectively).

3.6. Effect of temperature

The influence of temperature on TMP degradation was assessed by degrading the antibiotic solution at pH 4.5 in the presence of

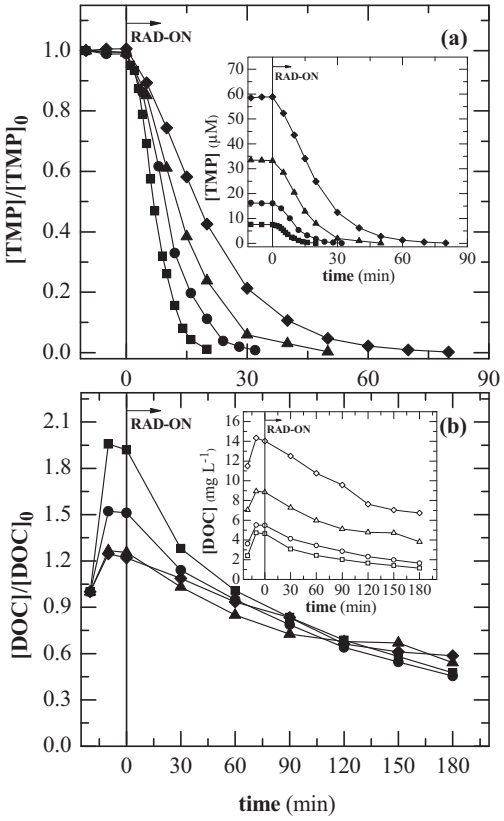

Fig. 6. Effect of TMP initial concentration on (a) normalized TMP concentration decay and (b) normalized DOC removal for the PEF degradation of TMP solutions in 50 mM Na_2SO_4 with 35.8 μM Fe^{3+} at pH = 4.5, 1:1 Fe(III)-to-citrate molar ratio, j = 5 mA cm^{-2}, 20 °C and flow rate of 40 L h^{-1}. $[TMP]_0$: (■) 6.9, (●) 17.2, (▲) 34.4 and (♦) 68.9 μM. The inset panels depict the corresponding TMP concentration decay and DOC removal in μM and mg L^{-1}, respectively.

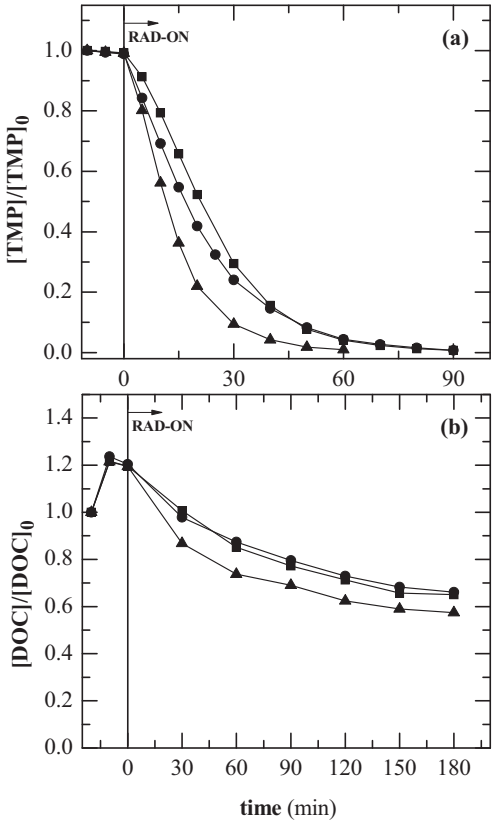

Fig. 7. Effect of temperature on (a) normalized TMP concentration decay and (b) normalized DOC removal for the PEF treatment of a 68.9 μM TMP solution in 50 mM Na_2SO_4 with 35.8 μM Fe^{3+} at pH = 4.5, 1:3 Fe(III)-to-oxalate molar ratio, j = 5 mA cm^{-2}, 20 °C and flow rate of 40 L h^{-1}. Temperature: (■, □) 10, (●, ○) 20 and (▲, △) 40 °C.

1:3 Fe(III)-to-oxalate molar ratio under the abovementioned conditions. Fig. 7 shows that the use of temperatures of 10 and 20 °C led to quite similar TMP and DOC decays and, in turn, the use of a greater temperature of 40 °C caused slightly faster TMP and DOC removals, with k_{TMP} and k_{DOC} values 1.7–1.8 and 2.2–2.5 times higher, respectively (see Tables 1 and 2). The beneficial effect of high temperatures on reaction kinetics in Fenton's based processes has been largely attributed to a higher Fe^{3+} reduction through thermal reactions as Eqs. (12)–(14) [8,56].

$$Fe^{3+} + H_2O_2 \rightarrow Fe^{2+} + HO_2^{\bullet} + H^+ \quad (12)$$

$$Fe^{3+} + HO_2^{\bullet} \rightarrow Fe^{2+} + O_2 + H^+ \quad (13)$$

$$Fe^{3+} + O_2^{\bullet -} \rightarrow Fe^{2+} + O_2 \quad (14)$$

The current study wanted to go further and examined the influence of temperature on the amount of the photoactive species in solution. To do this, the molar fractions of the most photoactive species, in terms of Fe^{3+} total concentration, were calculated by the chemical equilibrium modeling system MINEQL+ [52] under the initial conditions in the presence of oxalate, Fe^{3+}, Na_2SO_4 and chloride (see Fig. 8a) and under the same settings but in the absence of oxalate ion (see Fig. 8b), which corresponds to the system after total photodecarboxylation of Fe(III)–oxalate complexes. As can be seen, at the starting conditions quite similar molar fractions of $Fe(ox)_2^-$ and $Fe(ox)_3^{3-}$ were obtained for all the temperatures in the overall pH range and after Fe(III)–oxalate complexes photodecarboxylation none photoactive species was available at pH 4.5. The slightly reaction enhancement at 40 °C can then be mainly associated with higher Fe^{2+} regeneration through the thermal reactions (12)–(14), and in minor proportion to the rise in rate of electrode reactions (1), (3) and (4) due to the faster mass transport toward/from the electrodes.

Moreover, an analysis at pH 2.8 (i.e. the pH value commonly assumed as optimal in light-induced Fenton's based processes) revealed increasing $FeOH^{2+}$ molar fractions together with temperature rise for the system in the absence of oxalate ion (see Fig. 8b) and in the absence of both oxalate ion and Na_2SO_4 (see Fig. 8c). Nevertheless, while the growth of the $FeOH^{2+}$ molar fraction in the former system was very poor ($FeOH^{2+}$ molar fractions of 2.7%, 3.8% and 6.9% for 10, 20 and 40 °C, respectively), in the latter one, common for photo-Fenton processes without electrolyte, the rise of the $FeOH^{2+}$ molar fraction was very accentuated ($FeOH^{2+}$ molar fractions of 14%, 22% and 40% for 10, 20 and 40 °C, respectively). Hence, the influence of temperature in light-induced Fenton's based processes at pH near 2.8 in the absence of high amounts of sulfate and carboxylic acids can be associated with the presence of different amounts of photoactive species besides of the occurrence of thermal reactions.

Despite of the better results found at high temperatures, their use should be taken carefully due to the existence of: (i) the quicker thermal decomposition of H_2O_2 into H_2O and O_2 (inactive species); (ii) the inefficient H_2O_2 decomposition through the thermal reactions (12)–(14) involved in the Fe^{3+} reduction, with the formation of less reactive species; and (iii) a significant water evaporation [57].

3.7. Role of different oxidizing species

As previously stated, •OH can be produced by electrochemical oxidation according to Eq. (1), Fenton's reaction (2) and photolysis of Fe(III)–hydroxy complexes thorough Eq. (5). In turn, the

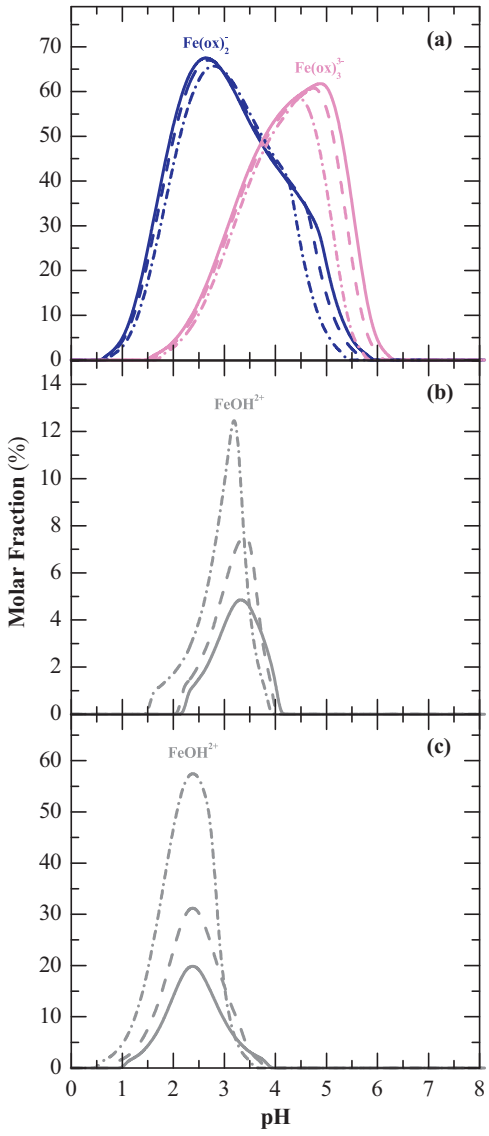

Fig. 8. Theoretical molar fraction of (a) $Fe(ox)_2^-$ and $Fe(ox)_3^{3-}$ and (b and c) $FeOH^{2+}$ species, regarding the total Fe^{3+} concentration, as a function of the solution pH at: (solid profile) 10 °C, (dash profile) 20 °C and (dash dot profile) 40 °C. Systems: (a) 107 μM oxalate ion (1:3 Fe(III)-to-oxalate molar ratio), 35.8 μM Fe^{3+}, 49.3 mM SO_4^{2-}, 98.6 mM Na^+ and 107 μM Cl^-, (b) absence of oxalate ion and (c) absence of oxalate ion and Na_2SO_4. Ionic strength of 148 and ~0 mM in the presence and absence of Na_2SO_4, respectively. Data were calculated from the chemical equilibrium modeling system MINEQL+ [52], using the equilibrium constants and enthalpies of Table SM-1 and including the formation of $Fe(OH)_{3(s)}$.

generation of other oxidizing species, the singlet oxygen ($^1O_2$), can occur from the excitation of the ground-state O_2 molecules in the presence of a sensitizer as is the case of TMP molecule and sub-structural moieties of TMP, 1,2,3-trimethoxybenzene (TMBz) and 2,4-diaminoprimidine (DAP), in pure water [58,59]. The role of these two oxidizing species was checked from the addition of selective scavenging agents like D-mannitol and sodium azide to quench •OH and $^1O_2$, respectively [60,61]. Each scavenger in 2 mM content was added to the 68.9 μM TMP solution in 50 mM Na_2SO_4 with 35.8 μM Fe^{3+} in the presence of 1:1 Fe(III)-to-citrate molar ratio at pH 4.5 and 20 °C to be further treated by PEF in the lab-scale flow plat at 5 mA cm^{-2} and flow rate of 40 L h^{-1}. Fig. 9 confirms the important role of •OH attack on TMP since the absence of this radical induced an inhibition of ca. 9.5 times in the k_{TMP} value (see Table 1). Surprisingly, the use of sodium azide led to an even slightly higher inhibition of TMP decay compared with D-mannitol,

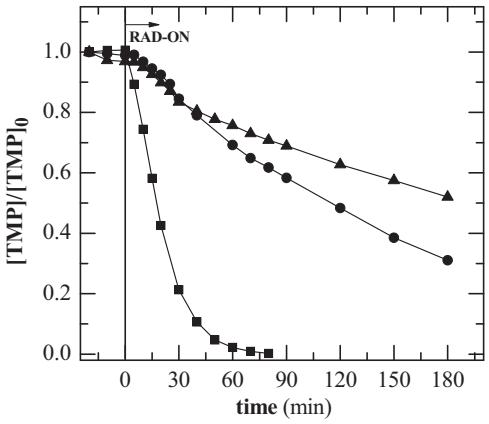

Fig. 9. Effect of (●) D-mannitol and (▲) sodium azide on normalized TMP concentration decay for the PEF degradation of a 68.9 μM TMP solution in 50 mM Na_2SO_4 with 35.8 μM Fe^{3+} at pH = 4.5, 1:1 Fe(III)-to-citrate molar ratio, j = 5 mA cm^{-2}, 20 °C and flow rate of 40 L h^{-1}. (■) Absence of scavenging agents.

with k_{TMP} 0.6 times inferior, pointing to a strong participation of $^1O_2$ in the degradation process. Although sodium azide has been mainly described as a high selective $^1O_2$ scavenger, some authors reported its non-selectivity since it can also react with •OH [62], which could better justify the results reported in Fig. 9.

3.8. Costs on carboxylate ligands

The selection of a carboxylate ligand should contemplate its price in order to minimize the global cost of the degradation process. Despite of the similar reaction kinetics found in PEF processes with 1:3 Fe(III)-to-oxalate and 1:1 Fe(III)-to-citrate and Fe(III)-to-tartrate molar ratios at pH 4.5, the prices on carboxylic acids considering the information supplied by *Quimitécnica.com—Comércio e Industria Química, SA* (Portugal) in January 2014 were ca. 28, 14 and 64 € per 1000 m^3 of solution for Fe(III)–oxalate, Fe(III)–citrate and Fe(III)–tartrate systems, respectively. Therefore, the use of citrate can be economically advantageous for the PEF treatment.

4. Conclusions

The PEF process with 1:3 Fe(III)-to-oxalate, 1:1 Fe(III)-to-citrate and 1:1 Fe(III)-to-tartrate molar ratios showed similar ability, both in terms of TMP and DOC decays, to degrade 20.0 mg L^{-1} (68.9 μM) TMP solutions in 50 mM Na_2SO_4 with 2.0 mg L^{-1} (35.8 μM) Fe^{3+} (Portuguese total iron discharge limit for WWTPs final effluents) at pH 4.5 and 20 °C using a lab-scale flow plant at 5 mA cm^{-2} and flow rate of 40 L h^{-1}. In contrast, the PEF method with 1:1 Fe(III)-to-malate molar ratio displayed inferior capacity to degrade TMP and its intermediates under similar conditions. 1:6 and 1:9 Fe(III)-to-oxalate molar ratios were needed to work at pH 5.0 and 5.5 with similar efficiencies to pH 4.5, respectively. Lower TMP removal rates were achieved when using smaller antibiotic concentrations. Moreover, the use of various temperatures proved that the regeneration of Fe^{2+} through thermal reactions plays a poor role in PEF processes mediated by Fe(III)–oxalate complexes. On the other hand, the beneficial effect of temperature in light-induced Fenton's based processes at pH near 2.8 in the absence of high amounts of Fe(III)–carboxylate complexes and sulfate ion can be strongly related to the presence of increasing amounts of $FeOH^{2+}$ species. The use of scavengers has confirmed that the TMP degradation in the PEF process can be mainly attributed to the action of •OH. Low amounts of oxalic, oxamic and formic acids were generated during all the PEF processes with Fe(III)–carboxylate complexes, being

almost completely removed at the end of the TMP treatments. Ferric speciation diagrams demonstrated to be a good tool to elucidate the behavior of the PEF process mediated by Fe(III)–carboxylate complexes.

Acknowledgments

Financial support was partially provided by (i) project PEst-C/EQB/LA0020/2013, financed by FEDER through COMPETE—*Programa OperacionalFactores de Competitividade*, (ii) FCT—*Fundação para a Ciência e a Tecnologia*, (iii) QREN and (iv) ON2. F.C. Moreira acknowledges her Doctoral fellowship SFRH/BD/80361/2011 supported by FCT. V.J.P. Vilar acknowledges the FCT Investigator 2013 Programme (IF/01501/2013).

Appendix A. Supplementary data

Supplementary data associated with this article can be found, in the online version, at http://dx.doi.org/10.1016/j.apcatb.2014.06.008.

References

[1] L.C. Almeida, S. Garcia-Segura, C. Arias, N. Bocchi, E. Brillas, Chemosphere 89 (2012) 751–758.
[2] F.C. Moreira, S. Garcia-Segura, V.J.P. Vilar, R.A.R. Boaventura, E. Brillas, Appl. Catal., B: Environ. 142–143 (2013) 877–890.
[3] N. Borràs, C. Arias, R. Oliver, E. Brillas, J. Electroanal. Chem. 689 (2013) 158–167.
[4] S. Garcia-Segura, L.C. Almeida, N. Bocchi, E. Brillas, J. Hazard. Mater. 194 (2011) 109–118.
[5] E.B. Cavalcanti, S. Garcia-Segura, F. Centellas, E. Brillas, Water Res. 47 (2013) 1803–1815.
[6] A. El-Ghenymy, N. Oturan, M.A. Oturan, J.A. Garrido, P.L. Cabot, F. Centellas, R.M. Rodríguez, E. Brillas, Chem. Eng. J. 234 (2013) 115–123.
[7] S. Garcia-Segura, E.B. Cavalcanti, E. Brillas, Appl. Catal., B: Environ. 144 (2014) 588–598.
[8] S. Malato, P. Fernández-Ibáñez, M.I. Maldonado, J. Blanco, W. Gernjak, Catal. Today 147 (2009) 1–59.
[9] E. Brillas, J.A. Garrido, R.M. Rodríguez, C. Arias, P.L. Cabot, F. Centellas, Port. Electrochim. Acta 26 (2008) 15–46.
[10] H.J.H. Fenton, J. Chem. Soc., Trans. 65 (1894) 899–910.
[11] E. Brillas, I. Sirés, M.A. Oturan, Chem. Rev. 109 (2009) 6570–6631.
[12] A. Dirany, I. Sirés, N. Oturan, A. Özcan, M.A. Oturan, Environ. Sci. Technol. 46 (2012) 4074–4082.
[13] A. Özcan, Y. Şahin, A.S. Koparal, M.A. Oturan, J. Hazard. Mater. 153 (2008) 718–727.
[14] I. Sirés, J.A. Garrido, R.M. Rodríguez, E. Brillas, N. Oturan, M.A. Oturan, Appl. Catal., B: Environ. 72 (2007) 382–394.
[15] S. Garcia-Segura, R. Salazar, E. Brillas, Electrochim. Acta 113 (2013) 609–619.
[16] E. Guinea, J.A. Garrido, R.M. Rodríguez, P.L. Cabot, C. Arias, F. Centellas, E. Brillas, Electrochim. Acta 55 (2010) 2101–2115.
[17] J.-J. Aaron, M.A. Oturan, Turk. J. Chem. 25 (2001) 509–520.
[18] Y. Sun, J.J. Pignatello, Environ. Sci. Technol. 27 (1993) 304–310.
[19] B.C. Faust, R.G. Zepp, Environ. Sci. Technol. 27 (1993) 2517–2522.
[20] O. Horváth, K.L. Stevenson, Charge Transfer Photochemistry of Coordination Compounds, VCH, New York, NY, 1992.
[21] A. Safarzadeh-Amiri, J.R. Bolton, S.R. Cater, Water Res. 31 (1997) 787–798.
[22] Y. Zuo, J. Hoigné, Environ. Sci. Technol. 26 (1992) 1014–1022.
[23] J.J. Pignatello, Environ. Sci. Technol. 26 (1992) 944–951.
[24] A. Safarzadeh-Amiri, J.R. Bolton, S.R. Cater, Sol. Energy 56 (1996) 439–443.
[25] M.R.A. Silva, W. Vilegas, M.V.B. Zanoni, R.F. Pupo Nogueira, Water Res. 44 (2010) 3745–3753.
[26] H.-J. Benkelberg, P. Warneck, J. Phys. Chem. 99 (1995) 5214–5221.
[27] J. De Laat, G. Truong Le, B. Legube, Chemosphere 55 (2004) 715–723.
[28] P. Neta, R.E. Huie, A.B. Ross, J. Phys. Chem. Ref. Data 17 (1988) 1027–1247.
[29] G.V. Buxton, C.L. Greenstock, W.P. Helman, A.B. Ross, J. Phys. Chem. Ref. Data 17 (1988) 513–886.
[30] H.B. Abrahamson, A.B. Rezvani, J.G. Brushmiller, Inorg. Chim. Acta 226 (1994) 117–127.
[31] E.M. Rodríguez, B. Núñez, G. Fernández, F.J. Beltrán, Appl. Catal., B: Environ. 89 (2009) 214–222.
[32] Y. Sun, J.J. Pignatello, J. Agric. Food. Chem. 40 (1992) 322–327.
[33] R.M. Smith, A.E. Martell, NIST Critically Selected Stability Constants of Metal Complexes Database Version 8.0 for Windows, Texas A&M University, United States, 2004.
[34] A.P.S. Batista, R.F.P. Nogueira, J. Photochem. Photobiol. A: Chem. 232 (2012) 8–13.
[35] I.N. Dias, B.S. Souza, J.H.O.S. Pereira, F.C. Moreira, M. Dezotti, R.A.R. Boaventura, V.J.P. Vilar, Chem. Eng. J. 247 (2014) 302–313.
[36] J. Burchall, in: J. Corcoran, F. Hahn, J.F. Snell, K.L. Arora (Eds.), Mechanism of Action of Antimicrobial and Antitumor Agents, Springer, Berlin, Heidelberg, 1975, pp. 304–320.
[37] A.J. Watkinson, E.J. Murby, D.W. Kolpin, S.D. Costanzo, Sci. Total Environ. 407 (2009) 2711–2723.
[38] B. Li, T. Zhang, Chemosphere 83 (2011) 1284–1289.
[39] F.C. Moreira, S. Garcia-Segura, R.A.R. Boaventura, E. Brillas, V.J.P. Vilar, Appl. Catal., B: Environ. 160–161 (2014) 492–505.
[40] W. Liu, S.A. Andrews, M.I. Stefan, J.R. Bolton, Water Res. 37 (2003) 3697–3703.
[41] R.F.P. Nogueira, M.C. Oliveira, W.C. Paterlini, Talanta 66 (2005) 86–91.
[42] ISO, ISO 6332:1988 Water Quality—Determination of iron—Spectrometric Method Using 1,10-Phenanthroline, 1998.
[43] N. Demirezen, D. Tarınç, D. Polat, M. Çeşme, A. Gölcü, M. Tümer, Spectrochim. Acta, A: Mol. Biomol. Spectrosc. 94 (2012) 243–255.
[44] A.C. Tella, J.A. Obaleye, Int. J. Chem. Sci. 8 (2010) 1675–1683.
[45] M.A. Sousa, C. Gonçalves, V.J.P. Vilar, R.A.R. Boaventura, M.F. Alpendurada, Chem. Eng. J. 198–199 (2012) 301–309.
[46] E.M. Glebov, I.P. Pozdnyakov, V.P. Grivin, V.F. Plyusnin, X. Zhang, F. Wu, N. Deng, Photochem. Photobiol. Sci. 10 (2011) 425–430.
[47] Y.-H. Huang, S.-T. Tsai, Y.-F. Huang, C.-Y. Chen, J. Hazard. Mater. 140 (2007) 382–388.
[48] C.F. Timberlake, J. Chem. Soc. (1964) 5078–5085 (resumed).
[49] Y. Zuo, J. Hoigné, Atmos. Environ. 28 (1994) 1231–1239.
[50] C. Sirtori, A. Agüera, W. Gernjak, S. Malato, Water Res. 44 (2010) 2735–2744.
[51] I. Michael, E. Hapeshi, V. Osorio, S. Perez, M. Petrovic, A. Zapata, S. Malato, D. Barceló, D. Fatta-Kassinos, Sci. Total Environ. 430 (2012) 167–173.
[52] W.D. Schecher, D.C. McAvoy, MINEQL+. A Chemical Equilibrium Modeling System, Version 4.6 for Windows, Environmental Research Software, Hallowell, ME, 2007.
[53] B.C. Faust, J. Hoigné, Atmos. Environ. A: Gen. Top. 24 (1990) 79–89.
[54] M.A. Oturan, M. Pimentel, N. Oturan, I. Sirés, Electrochim. Acta 54 (2008) 173–182.
[55] N.K. Vel Leitner, M. Doré, Water Res. 31 (1997) 1383–1397.
[56] A.Y. Sychev, V.G. Isak, Russ. Chem. Rev. 64 (1995) 1105–1129.
[57] B. Boye, M.M. Dieng, E. Brillas, Environ. Sci. Technol. 36 (2002) 3030–3035.
[58] X. Luo, Z. Zheng, J. Greaves, W.J. Cooper, W. Song, Water Res. 46 (2012) 1327–1336.
[59] C.C. Ryan, D.T. Tan, W.A. Arnold, Water Res. 45 (2011) 1280–1286.
[60] J. Bandara, J. Kiwi, New J. Chem. 23 (1999) 717–724.
[61] J.M. Monteagudo, A. Durán, I. San Martin, A. Carnicer, Appl. Catal., B: Environ. 106 (2011) 242–249.
[62] X. Zhang, B.S. Rosenstein, Y. Wang, M. Lebwohl, H. Wei, Free Radical Biol. Med. 23 (1997) 980–985.